Nanoscale Depth-Resolved Coherent Femtosecond Motion in Laser-Excited Bismuth

S. L. Johnson,[1,*] P. Beaud,[1] C. J. Milne,[2] F. S. Krasniqi,[1] E. S. Zijlstra,[3] M. E. Garcia,[3] M. Kaiser,[1] D. Grolimund,[1] R. Abela,[1] and G. Ingold[1]

[1]*Paul Scherrer Institut, CH-5232 Villigen PSI, Switzerland*

[2]*Laboratoire de Spectroscopie Ultrarapide, Ecole Polytechnique Fédérale de Lausanne, CH-1015 Lausanne, Switzerland*

[3]*Theoretische Physik, Universität Kassel, Heinrich-Plett-Strasse 40, 34132 Kassel, Germany*

(Received 4 October 2007; published 14 April 2008)

We employ grazing-incidence femtosecond x-ray diffraction to characterize the coherent, femtosecond laser-induced lattice motion of a bismuth crystal as a function of depth from the surface with a temporal resolution of 193 ± 8 fs. The data show direct consequences on the lattice motion from carrier diffusion and electron-hole interaction, allowing us to estimate an effective diffusion rate of $D = 2.3 \pm 0.3$ cm^2/s for the highly excited carriers and an electron-hole interaction time of 260 ± 20 fs.

DOI: 10.1103/PhysRevLett.100.155501 PACS numbers: 61.80.Ba, 61.05.C−, 63.20.K−, 78.47.J-

Excitation of a solid with an ultrafast optical pulse can create conditions far from thermal equilibrium, providing unique opportunities to explore interaction between electronic, magnetic, and atomic subsystems. The resulting dynamics typically involves atomic motion over a wide range of length scales, ranging from picometers to nanometers. Recently, considerable attention has focused on the femtosecond lattice dynamics of high amplitude coherent phonons in laser-excited bismuth [1–4].

Under standard conditions, bismuth crystallizes in the A7 structure as a rhombohedral unit cell with a two atom basis. Each basis atom is positioned along the body diagonal of the unit cell at $\pm zc$ from a fixed lattice point, where $c = 1.18$ nm is the length of the body diagonal and $z = 0.2334$ [5]. This can be considered as a small distortion of a simple cubic structure, stabilized into a lower-symmetry structure by the formation of a highly restricted density of electronic states near the Fermi energy [6]. The distortion is sensitive to electronic excitation. In particular, excitation by a femtosecond laser pulse shifts the equilibrium position of the atomic position parameter z toward $z = 0.25$, resulting in a coherent A_{1g} optical phonon as the atoms oscillate about their new equilibrium positions [7–9].

Most observations of the coherent A_{1g} mode in bismuth are based on measuring small changes in the reflectivity of the surface. Since the dielectric function of the crystal depends on its underlying structure, the dynamics of the unit cell structure result in a modulation of the reflectivity. As useful as these measurements are, they provide only rough estimates of the actual magnitude of interatomic motion. As a way to improve the accuracy of these estimates, pioneering femtosecond x-ray diffraction measurements have measured quantitatively the volume-averaged amplitude of the A_{1g} mode in a 50 nm thick, (111)-oriented film of crystalline bismuth [2,4]. The observed changes in the integrated intensity of the (111) and (222) diffraction peaks are directly related to the average separation of the basis atoms, providing a spatially integrated view of the dynamics of the unit cell over the entire film thickness.

To more completely characterize the dynamics of bismuth both spatially and temporally, we employ grazing-incidence, highly asymmetric x-ray diffraction to study the femtosecond structural changes of a bismuth crystal as a function of depth from the surface. Femtosecond x-ray pulses are created using the synchrotron electron-beam slicing method [10] as implemented at the Swiss Light Source [11]. The 140 ± 30 fs x-ray pulses are focused onto the sample by two optical elements. First, a horizontally mounted grazing-incidence toroidal mirror collimates the x rays vertically and creates a weak horizontal focus of 250 μm at the sample position. The second element is an elliptically bent single mirror placed 43 cm before the sample, focusing the beam vertically to a size <10 μm. Just before the sample, a Mo/B_4C multilayer mirror ($\gamma = 0.5$, 25 Å period) deflects the beam horizontally, selecting an x-ray energy of 7.15 keV with a bandwidth of 1.2%.

The sample under investigation is a single crystal of bulk bismuth, with one surface cut and polished to the (411)-orientation. We excite the near-surface region of the crystal with a femtosecond laser "pump" pulse incident on the sample at a grazing angle of 15° (π-polarization). After a variable delay set by an optical delay line in the pump beam, the x-ray "probe" beam (180 photons/pulse at 1 kHz) enters the crystal with vertical grazing incidence $\alpha = 0.4$–$2.0°$. An avalanche photodiode measures the noncoplanar diffracted intensity from the (111) lattice planes after optimization of the diffraction by rotating the sample about its surface normal.

By measuring time-resolved changes in the diffracted x-ray intensity for different values of the incidence angle α, we observe the laser-induced unit cell structure changes as a function of depth into the crystal. To understand the relationship between α and probe depth, consider Bragg diffraction from a perfect crystal when the angle θ between the exit beam and the surface is much larger than the critical angle for external reflection. The total wave field amplitude at a point $\mathbf{r}$ inside the crystal is [12]

$$D(\mathbf{r}) = D_0 \exp(ik_0 ux) \exp(i\mathbf{k}_{0\|} \cdot \mathbf{r}_\|) + D_h \exp[ik_0(u - \psi)x] \exp[i(\mathbf{k}_0 + \mathbf{h})_\| \cdot \mathbf{r}_\|]. \quad (1)$$

Here D_0 and D_h are amplitudes corresponding to the incident and diffracted wavefields, respectively, $\mathbf{k}_0$ is the incoming wave vector, x is the distance from the surface of the crystal, $\mathbf{h}$ is the reciprocal lattice vector, $\psi = -2\sin\theta_B \sin\phi$, θ_B is the Bragg angle, and ϕ is the angle between $\mathbf{h}$ and the surface. The subscript $\|$ indicates projection onto the surface plane. The dimensionless, complex-valued parameter u is the x component of the forward-diffracted wave vector inside the crystal, normalized by k_0. It is given by the solution to the third-order dispersion equation

$$(u^2 - \gamma_0^2 - \chi_0)(u + \psi + \sqrt{\gamma_h^2 + \chi_0}) = \frac{P^2 \chi_h \chi_{\bar{h}}}{2|\gamma_h|}, \quad (2)$$

subject to the condition that $\mathrm{Im}[u] > 0$, where $\gamma_0 = \sin\alpha$, $\gamma_h = -\sin\theta$, P is a polarization factor ($P = 1$ for σ- and $P = \cos 2\theta_B$ for π-polarization), and the quantities χ_0, χ_h and $\chi_{\bar{h}}$ are Fourier components of the x-ray susceptibility. Inspection of Eq. (1) shows that the wave field is proportional to $\exp(-x/L)$, with attenuation length $L = 1/k_0 \mathrm{Im}[u]$. The value of L decreases dramatically with α, ranging from 160 nm for $\alpha = 2.0°$ to 7.6 nm for $\alpha = 0.4°$ when evaluated at the Bragg peak.

Figure 1 shows the normalized diffracted intensity from the sample as a function of pump-probe delay time for different grazing-incidence angles, with an absorbed excitation fluence of 1.1 ± 0.1 mJ/cm^2. The A_{1g} oscillations are clearly visible. As the angle increases the probe depth also increases, and the relative change in the diffracted intensity decreases. There are also noteworthy changes in the general shape of the curves, indicating a depth dependence to the structural evolution. Figure 2 shows the dependence of the dynamics on absorbed excitation fluence F_{abs} for $\alpha = 0.45°$ ($L = 14$ nm at the Bragg peak). In agreement with earlier work [1,4], the average frequency ν of the coherent oscillations decreases nearly linearly with increasing fluence; the inset to Fig. 2 shows a fit to the function $\nu = \nu_0 - bF_{\mathrm{abs}}$, where $\nu_0 = 2.92$ THz is the frequency measured for very low fluence excitation [1] and b is estimated by the fit as 0.201 ± 0.002 THz cm^2/mJ. This frequency shift is mostly due to flattening of the interatomic potential surface [3].

By employing an iterative analysis on the angle-dependent data we can estimate the depth- and time-dependent atomic position parameter $z(x, t)$ [13]. The results summarized in Fig. 3 show the importance of resolution in x for accurately characterizing the structural response. Most apparently, the largest changes in z occur for $x < 25$ nm. Within the first 25 nm from the surface, there are marked differences between the behavior of z for $x < 7.5$ nm and for 15 nm $< x <$ 25 nm: near the surface, the quasiequilibrium value of z appears to decay monotonically after the initial excitation, whereas for the deeper layer the average value of z increases over the first 600 fs to approximately the same level as that of the near-surface region. The raw angle data in Fig. 1 show similar behavior for $\alpha > 0.45°$, indicating that in fact the average displacement of z for the entire probed depth of the crystal ($x < 150$ nm) increases over this time interval. For the

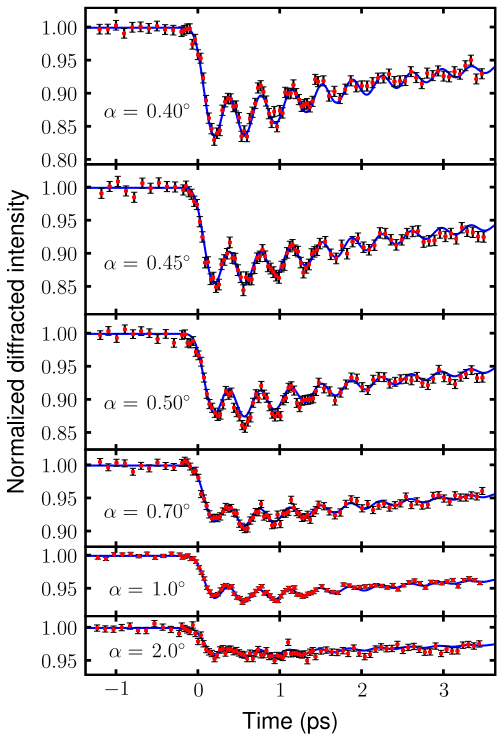

FIG. 1 (color online). Time-resolved diffraction at 1.1 mJ/cm^2 absorbed fluence for different values of the x-ray grazing-incidence angle α: experimental data (symbols) and the results from the fit discussed in the text (line).

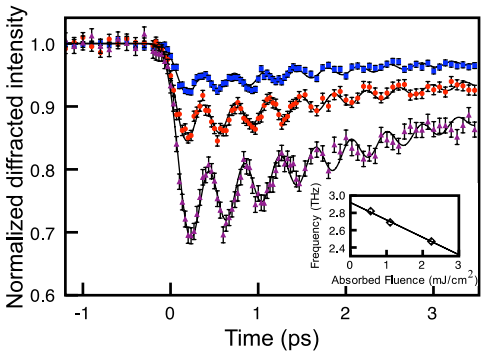

FIG. 2 (color online). Dependence of the dynamics of the diffracted intensity on absorbed fluence with $\alpha = 0.45°$: 0.56 mJ/cm^2 (blue squares), 1.10 mJ/cm^2 (red circles), and 2.24 mJ/cm^2 (purple triangles). The curves are fits of each data set to a simple model of displacive excitation assuming a constant phonon frequency, linear damping and an exponential relaxation of the equilibrium distance between basis atoms [8]. The inset shows the oscillation frequency as a function of fluence as well as a fit of this data to a line as described in the text. The uncertainty in the absolute values of fluence is estimated at $\pm 10\%$; the relative values are accurate to $\pm 2\%$.

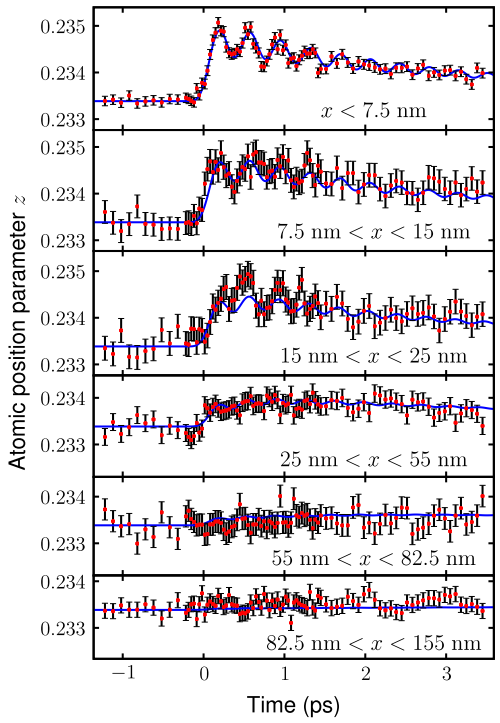

FIG. 3 (color online). Depth-dependence of the atomic position parameter z: after two iterations of the algorithm discussed of Ref. [13] (circles) and the results of the fit discussed in the text (line).

very deep layers of the crystal ($x > 25$ nm) the change in z is small, showing an increase from $0 < t < 1$ ps and then remaining approximately constant until the end of the data window.

Within the displacive excitation model [8], both the generation of the coherent A_{1g} phonon population and the changes in the observed average value of z are driven parametrically by z_{eq}, the quasiequilibrium value of z. The changes in z_{eq}, which can occur much faster than a phonon period, are driven by electronic excitation and relaxation. We assume that the energy of the laser pulse is absorbed in the crystal over an exponential depth profile with absorption length L_0. The initial energy distribution of carriers is highly nonthermal, but carrier-carrier scattering mechanisms will act to very quickly redistribute the carriers. In the case of semimetallic bismuth, however, the highly restricted density of states near the Fermi energy slows the interaction between the electron and holes to an estimated 1 ps time scale [14], much slower than in a true metal. All-electron density functional theory (DFT) calculations similar to those outlined in Ref. [15] have been used to compare values of Δz_{eq}, the change in the quasiequilibrium value of z, under two alternate scenarios: (i) a ''single-chemical potential model'', where the electron and hole subsystems are completely thermalized into a single Fermi-Dirac distribution, and (ii) a ''two-chemical potential model'', where the electron and hole subsystems are independent and separately thermalized into two Fermi-Dirac distributions. For each case we may approximate Δz_{eq} as proportional to the carrier energy density n for the small perturbations observed in this experiment: $\Delta z_{\mathrm{eq}} \approx a_1 n$ for the single-chemical potential model and $\Delta z_{\mathrm{eq}} \approx a_2 n$ for the two-chemical potential model. The values of a_1 and a_2 are very different ($a_2/a_1 = 0.58$). For times >1 ps, the single-chemical potential model seems to most accurately describe key features of the lattice dynamics [15]. We expect, then, that interaction between the electron and hole subsystems has a large impact on the lattice motion observed in our measurements.

We now construct a very simple two-fluid model of the spatiotemporal evolution of the energy in the carriers (electrons + holes). Let n_1 and n_2 denote the energy density of carriers that satisfy the assumptions of the single-chemical potential model and the two-chemical potential model, respectively. We assume that n_1 and n_2 satisfy the set of partial differential equations

$$\frac{\partial n_1}{\partial t} = D\frac{\partial^2 n_1}{\partial x^2} - n_1/\tau_1 + n_2/\tau_2, \tag{3}$$

$$\frac{\partial n_2}{\partial t} = D\frac{\partial^2 n_2}{\partial x^2} - n_2/\tau_1 - n_2/\tau_2, \tag{4}$$

where D is a constant diffusivity, τ_1 is the time scale for thermal equilibration of the carriers with the lattice, and τ_2 is the time for thermal equilibration between the electrons and holes (redistribution of carriers into the single-chemical potential model). The initial conditions at $t = 0$ for $x > 0$ are $n_1(x, 0) = 0$ and $n_2(x, 0) = n_0 e^{-x/L_0}$, where $n_0 = F_{\mathrm{abs}}/L_0$ is the density of the absorbed laser energy at the surface. Since carrier energy cannot diffuse through the surface of the crystal, we employ the Neumann boundary conditions $(\partial n_1/\partial x)_{x=0} = (\partial n_2/\partial x)_{x=0} = 0$.

Closed-form solutions for $x, t > 0$ are

$$n_1(x, t) = n_0 e^{-t/\tau_1}(1 - e^{-t/\tau_2})h(x, t), \tag{5}$$

$$n_2(x, t) = n_0 e^{-(1/\tau_1 + 1/\tau_2)t} h(x, t), \tag{6}$$

$$h(x, t) = \frac{2}{\pi}\int_0^\infty \frac{1}{1 + s^2} e^{-Ds^2 t/L_0^2} \cos(sx/L_0) ds. \tag{7}$$

Taking $z_0 = 0.2334$ as the ground state equilibrium value of z [5], the quasiequilibrium atomic position parameter is $z_{\mathrm{eq}}(x, t) = z_0 + a_1 n_1(x, t) + a_2 n_2(x, t)$, which simplifies to

$$z_{\mathrm{eq}}(x, t) = z_0 + \frac{A}{L_0} e^{-t/\tau_1}(1 - f e^{-t/\tau_2})h(x, t) \tag{8}$$

for $A = F_{\mathrm{abs}} a_1$ and $f = 1 - a_2/a_1$. To find $z(x, t)$ we solve

$$\frac{\partial^2 z}{\partial t^2} = -4\pi^2[\nu_0 - (z_{\mathrm{eq}} - z_0)\beta]^2(z - z_{\mathrm{eq}}) - \gamma\frac{\partial z}{\partial t}, \tag{9}$$

where β is a constant representing the softening of the mode under electronic excitation, γ is a damping coefficient representing the decay of the A_{1g} mode, and $z(x, t) = z_0$ for $t < 0$. This form assumes that the softening of the A_{1g} mode is a linear function of z_{eq}, which seems reasonable in view of the fluence dependence results depicted in

the inset of Fig. 2. Once we have determined $z(x, t)$ we then calculate the diffracted x-ray intensity for different values of the incidence angle α as described in Ref. [13] by representing the x dependence of $z(x, t)$ as a series of layers with thickness $\Delta x = 2.5$ nm. The temporal resolution of the experiment is approximated by convolution with a Gaussian with full-width-at-half-maximum τ_{fwhm}.

The results of a least-squares fit of this model to the data are plotted as solid curves in Fig. 1, and the average behavior of $z(x, t)$ over the various depth-intervals are shown in Fig. 3. The p value of the fit is 0.24 and the curves are largely consistent with the data, with the largest residuals occurring at $t \approx 0.5$ ps for $\alpha = 0.50°$ and 15 nm $< x <$ 25 nm. We estimate values for the absorption length $L_0 = 26 \pm 2$ nm, the diffusion constant $D = 2.3 \pm 0.3$ cm^2/s, the electronic energy decay time $\tau_1 = 7.6 \pm 0.6$ ps, the electron-hole thermalization time $\tau_2 = 260 \pm 20$ fs, the parameter $f = 0.53 \pm 0.06$, the A_{1g} mode softening parameter $\beta = 248 \pm 7$ THz, the integrated amplitude parameter $A = 56.0 \pm 1.0$ pm, the coherent phonon damping rate $\gamma = 1.01 \pm 0.11$ ps^{-1}, and the time resolution $\tau_{\mathrm{fwhm}} = 193 \pm 8$ fs. The fitted value of L_0 is somewhat higher than the 16 nm optical absorption coefficient measured via ellipsometry. The result for the diffusivity D is much lower in magnitude compared against the 100 cm^2/s ground state ambipolar diffusivity estimated from the room temperature mobilities of electrons and holes along the inward surface normal (2.3 and 0.5 m^2 V^{-1} s^{-1}, respectively) [16], suggesting that the effective diffusivity changes drastically upon strong electronic excitation. A similar effect was observed in models of diffusive transport applied to A_1 phonons in tellurium, where the fitted diffusivity for electronically excited tellurium was 10 cm^2/s rather than the 40 cm^2/s estimated from ground state properties [17]. In the case of bismuth this decrease may be more pronounced due to carrier confinement combined with the strong quantum size effects on carrier transport that can cause a several orders of magnitude drop in carrier mobility in films with thickness comparable to L_0 [18]. Our value of D is close to the 5 cm^2/s diffusivity cited for a similar model of excited A_{1g} phonons in 100 nm bismuth films [19]. A more refined model of carrier interaction and transport that takes into explicit account the effects of carrier confinement and variable diffusivity could give a more accurate description of the dynamics, but even so our simple model with a constant diffusivity appears to work reasonably well.

Our fitted values for f, β and $a_1 = A/F_{\mathrm{abs}} = (0.51 \pm 0.05) \times 10^{-5}$ cm^3/J may be compared against the results of the DFT calculations. The value of f from the DFT calculations is 0.42, close to the fitted value of 0.53 ± 0.06. The DFT calculations also predict $\beta = 230$ and 157 THz for the single- and two-chemical potential models, respectively. Since $\tau_2 < 1/\nu_0$, it is more appropriate to compare the value for the single-chemical potential model to the fit results, and indeed the values are close. The DFT-derived value for a_1 is 0.77×10^{-5} cm^3/J, which is somewhat higher than that obtained from the fits and consistent with the general trend of the local density approximation to underestimate band gaps.

As illustrated by the case of femtosecond laser-excited bismuth, the additional information on the depth dependence of the lattice response provided by femtosecond grazing-incidence x-ray diffraction is highly useful in extracting critical, quantitative information on the effects of carrier transport, electron-hole interaction, and relaxation that can be compared against models. This information is difficult to obtain by other means, and it is fundamental to understanding the structural evolution of materials driven strongly out of thermal equilibrium. Beyond the numerous materials in which large amplitude laser generated coherent phonons have been observed with optical methods [20], there is interest in using ultrafast lasers to drive potentially useful phase transitions in strongly correlated crystalline solids [21]. The technique introduced here can be a useful tool to understand the structural evolution of these materials with spatial resolution over the entire excitation depth, ultimately facilitating these efforts.

We gratefully acknowledge C. Borca for experimental support. This work was performed at the Swiss Light Source, Paul Scherrer Institut, Villigen, Switzerland.

*Steve.Johnson@mailaps.org

[1] M. Hase *et al.*, Phys. Rev. Lett. **88**, 067401 (2002).
[2] K. Sokolowski-Tinten *et al.*, Nature (London) **422**, 287 (2003).
[3] E. D. Murray *et al.*, Phys. Rev. B **72**, 060301(R) (2005).
[4] D. M. Fritz *et al.*, Science **315**, 633 (2007).
[5] P. Fischer, I. Sosnowska, and M. Szymanski, J. Phys. C **11**, 1043 (1978).
[6] R. Peierls, *More Surprises in Theoretical Physics* (Princeton University Press, Princeton, New Jersey, 1991).
[7] T. K. Cheng *et al.*, Appl. Phys. Lett. **57**, 1004 (1990).
[8] H. J. Zeiger *et al.*, Phys. Rev. B **45**, 768 (1992).
[9] T. E. Stevens, J. Kuhl, and R. Merlin, Phys. Rev. B **65**, 144304 (2002).
[10] R. W. Schoenlein *et al.*, Science **287**, 2237 (2000).
[11] P. Beaud *et al.*, Phys. Rev. Lett. **99**, 174801 (2007).
[12] S. Stepanov and R. Köhler, J. Phys. D **27**, 1922 (1994).
[13] See EPAPS Document No. E-PRLTAO-100-042815. For more information on EPAPS, see http://www.aip.org/pubservs/epaps.html.
[14] M. Hase *et al.*, Phys. Rev. Lett. **93**, 109702 (2004).
[15] E. S. Zijlstra, L. L. Tatarinova, and M. E. Garcia, Phys. Rev. B **74**, 220301(R) (2006).
[16] G. A. Saunders and Z. Sumengen, Proc. R. Soc. A **329**, 453 (1972).
[17] P. Tangney and S. Fahy, Phys. Rev. B **65**, 054302 (2002).
[18] E. I. Rogacheva *et al.*, Appl. Phys. Lett. **82**, 2628 (2003).
[19] S. Fahy and D. A. Reis, Phys. Rev. Lett. **93**, 109701 (2004).
[20] R. Merlin, Solid State Commun. **102**, 207 (1997).
[21] M. Fiebig *et al.*, Science **280**, 1925 (1998).